Materials Today Advances 24 (2024) 100538

Contents lists available at ScienceDirect

Materials Today Advances

journal homepage: www.journals.elsevier.com/materials-today-advances/

Strain engineering: A sustainable alternative to avoid using strategic and critical raw materials in developing high-performance alloys

Swati Singh [a], Mingwen Bai [b], Allan Matthews [c], Shrikrishna N. Joshi [a,**], Saurav Goel [a,d,e,*]

[a] Department of Mechanical Engineering, Indian Institute of Technology Guwahati, Guwahati, 781039, India
[b] School of Mechanical Engineering, University of Leeds, Leeds, LS2 9JT, UK
[c] Henry Royce Institute, The University of Manchester, M13 9PL, UK
[d] School of Engineering, London South Bank University, 103 Borough Road, London, SE1 0AA, UK
[e] Mechanical and Aerospace Engineering, University of Petroleum and Energy Studies, Dehradun, 248007, India

ARTICLE INFO

Keywords:
Strain engineering
MPEAs
Sustainability/Net-zero goal

ABSTRACT

The quest to develop high-performance metallic alloys with properties superior to traditional alloys has driven scientists to synthesize numerous chemical alloy compositions over the past few decades. However, many of these compositions heavily depend on strategic and critical raw materials (S&CRMs), leading to significant environmental impacts due to intensive mining practices. Through this work, we present a scientific rationale to highlight that high performance in metal alloys can be achieved through strain engineering approach, which is a sustainable alternative to reduce the use of S&CRMs. Strain engineering refers to the process of deforming materials to induce changes in their microstructure, such as increasing dislocation density, promoting twinning, forming ultra-fine grained (UFG) or nano-crystalline (NC) structures, and in some cases, triggering phase transformations like transformation-induced plasticity (TRIP) and twinning-induced plasticity (TWIP) to enhance its properties. This encompasses conventional thermo-mechanical processing (TMP) methods, including rolling, forging, extrusion, and drawing, as well as advanced techniques commonly referred to as severe plastic deformation (SPD), such as High-Pressure Torsion (HPT), Equal Channel Angular Pressing (ECAP), Friction Stir Processing (FSP), and Twist Extrusion (TE).

Through a comprehensive data-driven analysis of pure elements and multi-principal element alloys (MPEAs), also known as high-entropy alloys (HEAs), we demonstrate that precise strain engineering techniques on alloys without S&CRMs can achieve mechanical properties well comparable to the S&CRMs based traditional alloys, suggesting a strong need of further research in this direction to eliminate the excessive reliance on S&CRMs. Furthermore, strain-engineered materials not only exhibit enhanced resistance to fatigue, corrosion, and wear but also offer significant weight saving. Even thinner strain-engineered materials outperform thicker traditional alloys in terms of performance. This study serves as a catalyst to revive interest in strain engineering and explore the ultimate potential of materials traditionally considered mechanically weak.

Nomenclature

AM	Additive Manufacturing
CCAs	Complex Concentrated Alloys
CIP	Cold Isostatic Pressing
CDRx	Continuous Dynamic Recrystallization
CRM	Critical Raw Material
DDRx	Discontinuous Dynamic Recrystallization
DED	Directed Energy Deposition

(*continued on next column*)

(*continued*)

DRV	Dynamic Recovery
EBM	Electron Beam Melting
ECAP	Equal Channel Angular Pressing
FSP/FSW	Friction Stir Processing/Friction Stir Welding
GA	Gas Atomization
GDRx	Geometric Dynamic Recrystallization
GND	Geometrically Necessary Dislocations
HAGB	High Angle Grain Boundary

(*continued on next page*)

* Corresponding author. School of Engineering, London South Bank University, London, SE10AA, UK.
** Corresponding author.
E-mail addresses: snj@iitg.ac.in (S.N. Joshi), GoeLs@Lsbu.ac.uk (S. Goel).

https://doi.org/10.1016/j.mtadv.2024.100538
Received 13 July 2024; Received in revised form 21 October 2024; Accepted 1 November 2024
Available online 8 November 2024

(*continued*)

HEAs	High Entropy Alloys
HIP	Hot Isostatic Pressing
HPT	High Pressure Torsion
HRSDR	High-Ratio Differential Speed Rolling
LAGB	Low Angle Grain Boundary
LENS	Laser Engineered Net Shaping
LMD	Laser Metal Deposition
L-PBF	Laser Powder Bed Fusion
MA	Mechanical Alloying
MDRx	Meta-Dynamic Recrystallization
MEA	Medium Entropy Alloy
MPEAs	Multi-Principal Element Alloys
NC	Nano-Crystalline
OER	Oxygen Evolution Reaction
ORR	Oxygen Reduction Reaction
PDA	Post-Deformation Annealing
PDRx	Post-Dynamic Recrystallization
P/M	Powder Metallurgy
S&CRMs	Strategic and Critical Raw Materials
SFE	Stacking Fault Energy
SLM	Selective Laser Melting
SPD	Severe Plastic Deformation
SPS	Spark Plasma Sintering
SSD	Statistically Stored Dislocations
TE	Twist Extrusion
TEM	Transmission Electron Microscopy
TMP	Thermo-Mechanical Processes
TWIP	Twinning-Induced Plasticity
TRIP	Transformation-Induced Plasticity
UFG	Ultrafine-Grained
UTS	Ultimate Tensile Strength
YS	Yield Strength

1. Introduction to the newly emerging multi-principal element alloys

High entropy alloys (HEAs) also known as multi-principal element alloys (MPEAs) or complex concentrated alloys (CCAs) have received critical attention due to their exceptional properties compared to conventional alloys. The superior properties of HEAs have been ascribed to four effects, namely, the high configurational entropy, severe lattice distortion, sluggish diffusion and synergistic cocktail effects.

Several HEAs are developed to overcome the strength-ductility conundrum, for example, CoCrFeMnNi HEA with fully recrystallized structure [1], $Al_{0.3}$CoCrFeNi HEA fibers [2] and TiZrHfNbTa HEA at cryogenic temperature [3] have all shown excellent strength-ductility combination. Various HEAs have also shown superior performance at elevated temperatures, demonstrating their potential to replace the traditional Ni- and Co-based superalloys as the next candidates to manufacture engine components [4,5]. These are also referred to as high-entropy superalloys (HESAs). Some HESAs that form γ and γ' phases, like conventional superalloys, include $Al_8Co_{17}Cr_{17}Cu_8Fe_{17}Ni_{33}$, $Al_8Co_{17}Cr_{14}Cu_8Fe_{17}Ni_{34.8}W_{0.1}Mo_{0.1}Ti_1$, $AlCoCrFeNi_{2.1}$, AlCoCrCuFeNi, and $Ni_{58.2}Al_{10}Co_{13.8}Cr_{6.3}Fe_{4.9}Ti_{6.8}$. Additionally, HESAs with positive lattice misfits such as $Al_{7.8}Co_{20.6}Cr_{12.2}Fe_{11.5}Ni_{40.7}Ti_{7.2}$, $Al_{10.3}Co_{17}Cr_{7.5}Fe_9Ni_{48.6}Ti_{5.8}Ta_{0.6}Mo_{0.8}W_{0.4}$ and $Al_{10.2}Co_{16.9}Cr_{7.4}Fe_{8.9}Ni_{47.9}Ti_{5.8}Mo_{0.9}Nb_{1.2}W_{0.4}C_{0.4}$, exhibit enhanced fatigue resistance due to slow glide-climb motion of dislocations along the γ/γ' interfaces, effectively hindering the propagation of fatigue cracks [4]. The equimolar TiZrHfNbTa HEA, composed of biocompatible elements, exhibits excellent mechanical properties, including a relatively low Young's modulus compared to the Ti–6Al–4V alloy, as well as superior biocompatibility and bio-corrosion resistance [6]. Various HEAs are also useful in hydrogen storage applications due to their large lattice distortion that provides more suitable interstitial sites for the occupation of hydrogen atoms compared to the conventional binary or ternary alloys. Examples of HEAs with strong hydrogen absorption/desorption properties include FeMnCoTiVZr, FeMnCrTiVZr, FeCrNiTiVZr, TiNbVZrHf, TiNbZrMoV and TiNbVZr [7]. Additionally, HEAs have shown great potential in oxygen evolution and reduction reactions (OER and ORR), which are at the heart of energy conversion technologies including fuel cells, metal-air (metal-oxygen) batteries and water-splitting. AlCoNiIrX (X = Mo, Cu, Cr, V, Nb), with reduced Ir content compared to the conventional Ir-based binary and ternary alloys, has demonstrated favorable OER characteristics, with AlCoNiIrMo exhibiting the highest OER activity and significantly enhanced cycling stability. Some HEAs, such as PtIrRuCuOs, AlNiCuPtPdAu, and AlCuNiPtMn, containing small amounts of precious elements, show enhanced activity toward ORR as well as superior long-term stability compared to commercial Pt/C [7]. Consequently, HEAs have emerged as superior alternatives to conventional alloys in various application sectors.

Developing high-performance MPEAs often relies on strategic and critical raw materials (S&CRMs) like Hf, Nb, Ta, W, Co, precious metals, and certain rare-earth elements to achieve superior properties. However, the growing scarcity of S&CRMs is becoming a major concern, and the extensive mining required to extract these materials poses a serious threat to global efforts to achieve Net Zero. To avoid technological stagnation and maintain progress, it is essential to develop alloys using abundant and more readily available resources. However, achieving the desired properties without using S&CRMs through conventional processing methods remains a significant challenge.

Classification of CRM is an important distinction here. Various CRMs reported to date by the European Union were classified in three categories (see Fig. 1). The **European Commission** regularly evaluates **S&CRMs** for the EU. These assessments, first introduced in 2011, are updated every three years to reflect evolving **industrial demand** and **supply risks**. Fig. 1 presents the materials included in these reports from 2011 to 2023.

We classified CRMs based on the frequency and continuity of their inclusion in these reports. Materials that have appeared in three or more reports and are still of concern in 2023 are categorized as **"1st Tier CRMs."** Recently identified materials, having appeared in two or fewer reports, are classified as **"2nd Tier CRMs."** Additionally, materials such as **Cr** and **indium (In)**, which are absent from the 2023 report, are classified as **"non-CRMs."** Fig. 1 also integrates SRMs, with hatched elements indicating those that are both **CRMs** and **SRMs.** These include **B/Borate, Bi, Co, Cu, Ga, Ge, Li, Mg, Mn, Ni, Si metal, Ti, and W.** Natural graphite, platinum group metals, and rare earth elements are also classified as both CRMs and SRMs, though they are absent from Fig. 1. Moreover, arsenic, baryte, coking coal, feldspar, fluorspar, strontium, and phosphate rock are also categorized as CRMs, but are likewise omitted from Fig. 1 [8].

1.1. Influence of manufacturing process on the mechanical properties

Through this work, a rationale was developed by analysing the reported mechanical properties, particularly yield strength (YS) of pure metals (Al, Cu, Mg, Ta, Ti, Fe, Ni) and MPEAs synthesized using different manufacturing methods. This comparison was designed to emphasize how different process conditions can be leveraged to achieve varying mechanical properties in a material—an aspect that has been significantly overlooked in literature.

(i) Mechanical deformation processes
- Thermo mechanical processes (TMP) such as rolling, forging, extrusion and drawing.
- Non-conventional TMP or Severe plastic deformation (SPD) processes such as High-Pressure Torsion (HPT), Equal Channel Angular Pressing (ECAP), Friction Stir Processing (FSP) and Twist Extrusion (TE).

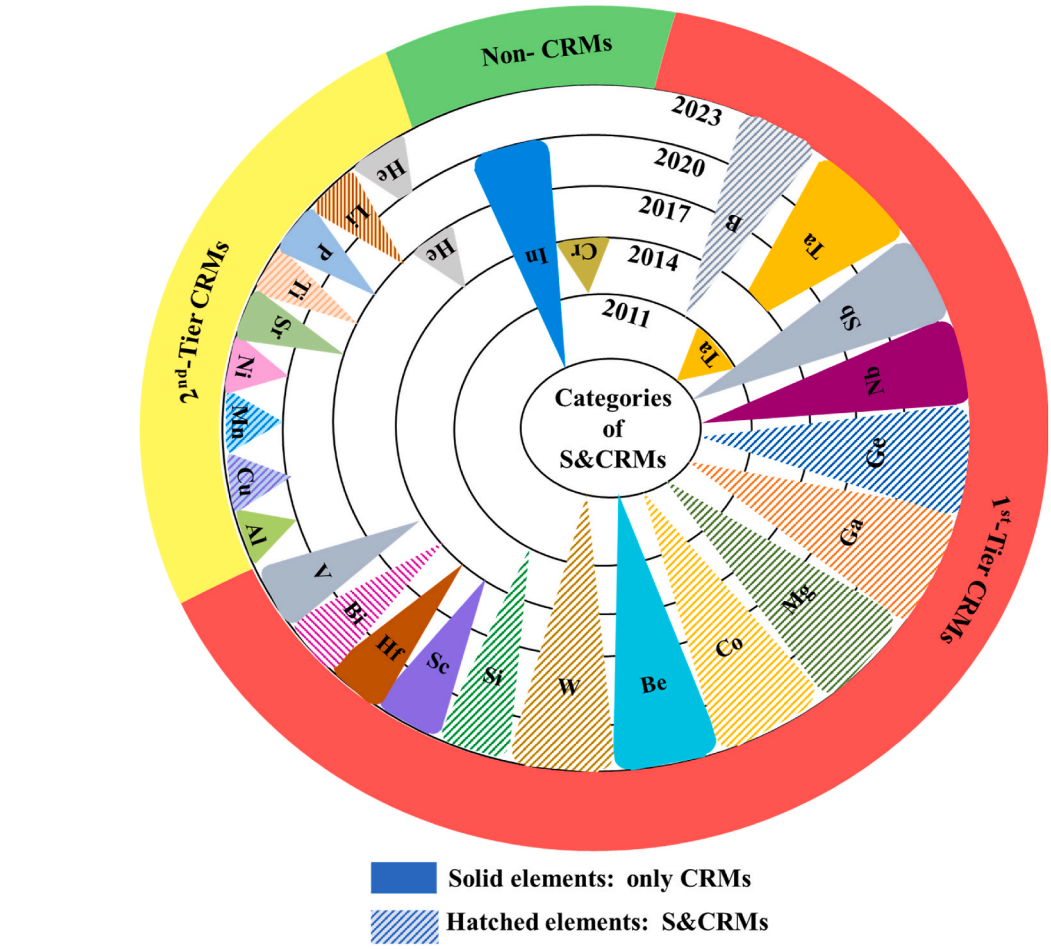

Fig. 1. Classification of various **Strategic and Critical Raw Materials (S&CRMs)** [8–13] (author's own contribution).

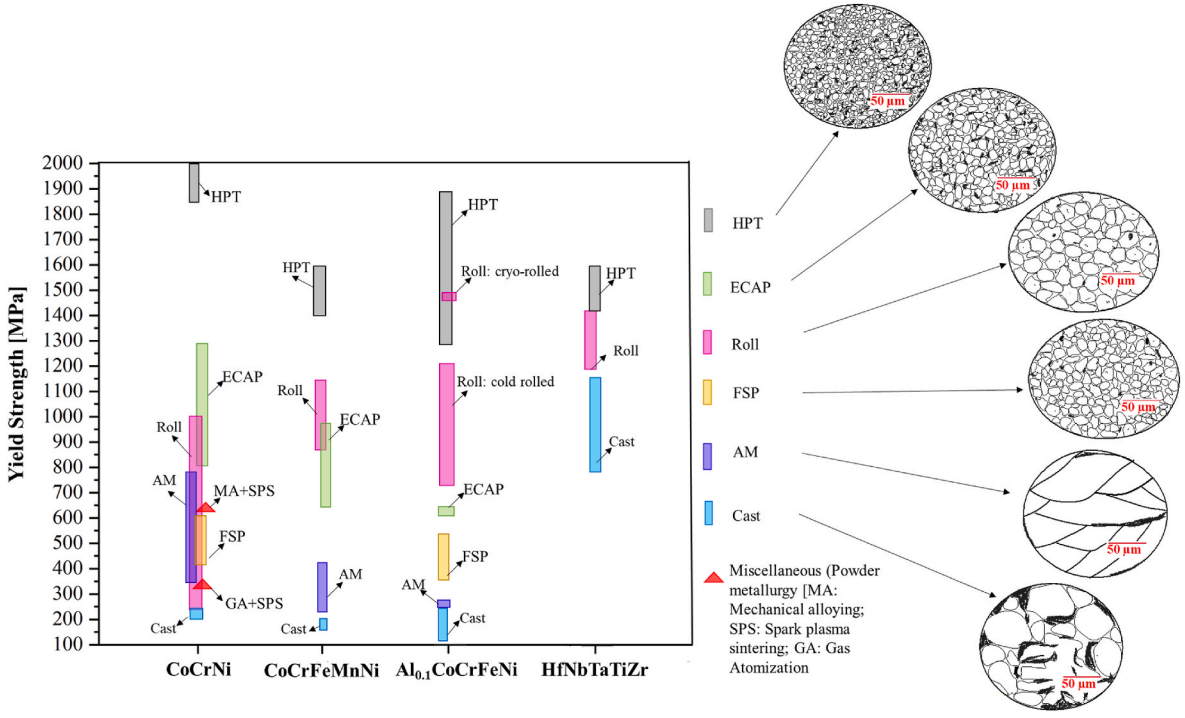

Fig. 2. Yield strength of four representative MPEAs showing the influence of processing route on the grain structure (author's own contribution).

(ii) Other manufacturing processes: Casting, powder metallurgy (P/M) and additive manufacturing (AM)

Fig. 2 presents a comparison of YS of four popular MPEAs CoCrNi, CoCrFeMnNi, $Al_{0.1}$CoCrFeNi and HfNbTaTiZr, showcasing the different mechanical properties based on the synthesis route. A detailed description of the manufacturing process, crystal structure, hardness, yield strength (YS), ultimate tensile strength (UTS), and elongation, as reported in the literature, can be found in Table 1s, provided as supplementary information. Although the YS of post-processed (heat-treated) samples are included in Table 1s, they were excluded from the preparation of Fig. 2. This is because the heat-treated samples typically exhibit increased ductility at the expense of strength.

Moreover, in certain experimental studies, tensile testing was not conducted, leading to missing information in the literature, and as a result, some data is unavailable for comparison in Fig. 2. For instance, the tensile test results of HfNbTaTiZr HEA processed through FSP, ECAP, AM and P/M have not been reported. Consequently, further experimental investigation of a wide range of MPEA compositions synthesized via diverse processing routes is indispensable to initiate a full-fledged exploration of strain engineering approaches in the synthesis of MPEAs/HEAs/CCAs.

As illustrated in Fig. 2, all four MPEAs processed via HPT exhibit higher YS, indicating that strain engineering can have a more pronounced effect on the mechanical properties (yield strength in this case). This suggests that strain engineering can be used to control the resulting mechanical properties in MPEAs, providing a compelling alternative to eliminate the need for the change of chemical composition.

CoCrFeMnNi HEA crystallizes in an FCC phase, and it was the first reported MPEA/HEA with excellent room-temperature ductility (~61.7 %–71 %) but relatively low YS (~209– 215 MPa) and UTS (~491–496 MPa). The grain size in this state typically ranges from approximately ~300–400 μm [14,15]. In contrast, when processed via High-Pressure Torsion (HPT), the CoCrFeMnNi alloy demonstrate a significantly higher YS (~1400 MPa) and UTS (~1740 MPa) at the expense of ductility, which dropped to 4 % with an ultra-fine grain (UFG) size of ~10 nm [16]. Post-deformation annealing (PDA) at 1073K for 1h of the HPT-processed CoCrFeMnNi HEA resulted in 80 % recovery of ductility, albeit, with a corresponding reduced YS of 530 MPa and UTS of 680 MPa and a grain size of ~4 μm.

The CoCrNi a medium entropy alloy (MEA) exhibits superior mechanical properties compared to its parent alloy, CoCrFeMnNi a high entropy alloy, irrespective of the processing route (see Fig. 2). When processed via HPT, the CoCrNi MEA demonstrates an exceptionally high YS of ~1880 MPa and UTS of around ~2170 MPa and a moderate ductility of ~9 % with a grain size of ~660 nm [17]. Schuh et al. [18] reported similar high YS (1901 ± 114 MPa) and UTS (2067 ± 153 MPa), though with a lower ductility (3.9 ± 1.5 %) for the HPT-processed CoCrNi MEA. Moreover, under cryogenic conditions, the HPT-processed CoCrNi alloy exhibit excellent strength and ductility (YS = 1975 MPa, UTS = 2054 MPa, and ductility = 27 %), outperforming its mechanical properties at room temperature (YS = 1435 MPa, UTS = 1580 MPa, and ductility = 24 %) [19]. This demonstrates that exceptional mechanical properties can be achieved with fewer constituent elements, indicating the potential for reduced use of chemical elements without negating the performance. CoCrNi contains less S&CRMs than its parent alloy CoCrFeMnNi and still exhibit superior mechanical properties, highlighting the scope of reduced use of S&CRMs.

The superior strength-ductility synergy of CoCrNi MEA compared to CoCrFeMnNi HEA has been attributed to its low stacking fault energy (SFE). The wider separation between Shockley partials in CoCrNi results in lower SFE, thereby enabling the activation of nano-twinning at significantly lower strains, both at room temperature and at cryogenic temperature. It is widely recognized that twin boundaries can enhance mechanical properties by increasing the strain hardening rate and delaying the onset of necking [20]. It should be noted that both CoCrFeMnNi and CoCrNi MPEA show strong temperature-dependent strength and ductility phenomena [19]. Otto et al. [21] highlighted the influence of temperature on the mechanical properties of CoCrFeMnNi HEA. They observed an improvement in strength from 763 MPa at room temperature to 1280 MPa at a cryogenic temperature (77K), along with an enhanced ductility from 50 % to 70 % for cold-rolled (~87 %) CoCrFeMnNi HEA.

Gludovatz et al. [22] reported improved strength and ductility (YS = 657 MPa, UTS = 1311 MPa, ductility = 0.9) for cold-forged and cross-rolled CoCrNi alloy at a reduced temperature of 77K. At room temperature, the YS and fracture toughness of CoCrFeMnNi HEA and CoCrNi MEA were found to be comparable, while the UTS and ductility of CoCrNi MEA were significantly higher than those of the CoCrFeMnNi HEA by 15 % and 30 %, respectively. However, at a cryogenic temperature of 77K, the UTS of both CoCrFeMnNi HEA and CoCrNi MPEA was comparable (~1300 MPa), but CoCrNi exhibited 27 % higher ductility and 25 % greater fracture toughness. Thus, it can be noticed that at room-temperature, the CoCrFeMnNi HEA suffers from a strength-ductility tradeoff. Post-processing heat treatment, such as annealing of ultrafine-grained (UFG) or nano-crystalline (NC) materials, help achieve a desirable balance of mechanical properties. However, this raises a key question: “Can the strength-ductility synergy be improved without heat treatment? To address this strength-ductility tradeoff, various strategies have been explored over the past few decades, including generating bimodal or heterogeneous microstructure [23], introducing nanotwins [24,25], and controlling twinning/-transformation induced plasticity (TWIP/TRIP) mechanism [26]. Picak et al. [27] demonstrated the formation of a desirable heterogeneous microstructure in the CoCrFeMnNi MPEA after two passes of ECAP at both high and medium temperatures, thereby eliminating the need for subsequent heat treatments. The resulting microstructure exhibited a bimodal/heterogeneous grain size distribution, characterized by two distinct regions: one with large, elongated grains, and the other consisting of recrystallized ultrafine grains (UFG). This heterogeneous structure facilitated a composite effect during plastic deformation, with the large grains enabling extended plasticity, while the smaller grains contributed to strengthening. Transmission Electron Microscopy (TEM) investigation revealed elongated UFGs, along with deformation twinning and ε-martensite lamellae, even after high-temperature deformation. Typically, dislocation plasticity serves as the primary deformation and strengthening mechanism in CoCrFeMnNi HEAs at room temperature. However, ECAP demonstrated significant potential for strengthening these materials by promoting grain refinement and increasing dislocation density. Notably, ECAP was shown to activate both Twinning-Induced Plasticity (TWIP) and Transformation-Induced Plasticity (TRIP), which substantially enhances the resistance to dislocation motion. The authors attributed the observed enhancement in strength and ductility to the simultaneous activation of twinning (TWIP) and ε-martensite (TRIP) mechanisms. This simultaneous activation of TWIP and TRIP in severely plastically deformed CoCrFeMnNi HEA was reported for the first time, warrants a more detailed investigation.

Furthermore, a superior combination of strength and ductility can be achieved in compositions exhibiting low stacking fault energy, primarily through the activation of nano-twinning mechanism, as previously demonstrated in the case of CoCrNi MEA. Thus, by processing materials to induce bimodal or heterogeneous microstructures, promoting nano-twins, controlling TWIP and TRIP mechanisms, or utilizing materials with inherently low SFE, eliminates the necessity of additional post-processing to achieve high strength-ductility synergy.

Moreover, akin to CoCrNi, which contains reduced S&CRMs compared to its parent CoCrFeMnNi, exhibiting superior mechanical properties, newer compositions without S&CRMs can be developed. Strain engineering approach inducing low-mobility defects, ultrafine grained structure (either homogeneous or heterogeneous, depending upon the specific requirements) and activating TWIP and TRIP mechanisms can be used. However, these strategies are primarily effective

under ambient conditions. Achieving a similar strength-ductility synergy in hydrogen-rich environments presents a significant challenge due to the susceptibility to hydrogen embrittlement. To address this issue, Mohammadi et al. [28] conducted HPT deformation on $Al_{0.1}CoCrFeNi$ alloy—an FCC-phase alloy noted for its sluggish hydrogen lattice diffusion. The HPT processing resulted in an impressive combination of high strength (YS = 1960 MPa) and ductility (10 %) through the generation of low-mobility lattice defects, such as nanotwins and Lomer-Cottrell locks. These defects act as hydrogen trapping sites, mitigating hydrogen-enhanced localized plasticity and minimizing stress concentration. Similarly, CoCrFeMnNi HEA processed via cold-rolling and annealing exhibited an excellent strength-ductility combination in hydrogen environments, with a significant improvement in resistance to hydrogen embrittlement due to grain refinement, which inhibited grain boundary decohesion [29]. Thus, by introducing various lattice defects—particularly low-mobility defects—and refining grain structures during TMP or SPD techniques, a desirable strength-ductility synergy can be achieved. This effect holds true in both ambient and hydrogen-exposed environments, especially for FCC-structured materials, which are known for their slow hydrogen lattice diffusion.

Aside from the study by Mohammadi et al. [28], there is a notable absence of research on the mechanical properties of HPT-processed $Al_{0.1}CoCrFeNi$ alloy in the literature. Therefore, it is crucial to conduct further experimental investigations on this alloy under HPT processing in absence of hydrogen to fully understand the unique influence of HPT processing on $Al_{0.1}CoCrFeNi$ alloy.

Similar to other compositions presented in Fig. 2, HPT processed HfNbTaTiZr HEA subjected to a shear strain (γ) > 40, exhibit a remarkable increase in strength, rising significantly from 830 MPa in its as-received state to 1900 MPa after deformation, primarily due to grain refinement. Surprisingly, despite substantial gain in strength, the specimen retained a notable degree of ductility, with only a minor reduction in total elongation at failure (from 9.2 % to 7.9 %). This retention of ductility was attributed to the dynamic deformation and recovery processes occurring at γ > 40, establishing a dynamic equilibrium of generation and annihilation of defects. This equilibrium resulted in a homogenous microstructure characterized by nanocrystalline, equiaxed grains. However, no conclusive evidence was found to attribute this enhancement to commonly known mechanisms, such as twinning or a bimodal grain size distribution, which are typically employed to achieve strength-ductility synergy. The underlying cause of the simultaneous improvement in strength and ductility remains unexplored, presenting a promising avenue for future research [30].

Furthermore, given the high YS observed in HPT-deformed MPEAs across various compositions, it becomes imperative to investigate whether similar trends extend to pure elements or if this observation is exclusive to MPEAs. To address this question, more data was extracted from literature for several pure elements (Al, Cu, Mg, Ni, Ta, Ti, Fe). A comprehensive description of each element's processing conditions, crystal structure, hardness, yield strength, ultimate tensile strength, and elongation, as reported in the literature, is provided in Supplementary Table 2s. However, only a limited number of studies report YS for specific pure elements across all processing routes (see Fig. 3).

Except for Al and Cu, a similar trend to that observed in MPEAs was also noted for pure elements, where the YS of samples processed via high-pressure torsion (HPT) consistently exceeded that of samples produced through other processing methods (see Fig. 3). Notably, ECAP processed Al exhibited a slightly higher YS of 173 MPa after 10 ECAP passes, compared to 146 MPa for HPT-processed Al at an equivalent strain of 25.1. This may be attributed to the higher stresses exerted during ECAP compared to HPT.

Fig. 4 highlights the effect of TMP/SPD processing on microsturucture of an alloy/element. Both processes, namely ECAP and HPT, induce severe plastic deformation but differ in the nature of the stresses involved. ECAP applies shear stress uniformly as the material passes through a die with an angular channel, leading to grain refinement and enhanced mechanical properties. It induces more homogeneous deformation across larger samples. HPT, on the other hand, imposes intense compressive and torsional stresses by subjecting the material to high pressure while rotating, resulting in extreme grain refinement, particularly near the sample's edges. HPT generally produces higher dislocation densities compared to ECAP.

In the case of pure Cu, the YS of HPT-deformed samples vary in the range of 370–474 MPa, the highest among all processing methods, except for cryo-rolled pure Cu, which exhibits YS ranging from 336 to 520 MPa. The increase in YS could be linked to the operating temperature, where rolling was carried out at cryogenic temperature, which enhances material's strength.

Regarding pure Ta, the YS of HPT-processed samples could not be displayed in Fig. 3, as only a single study provided data on the UTS of HPT-processed Ta without corresponding YS data [31]. For

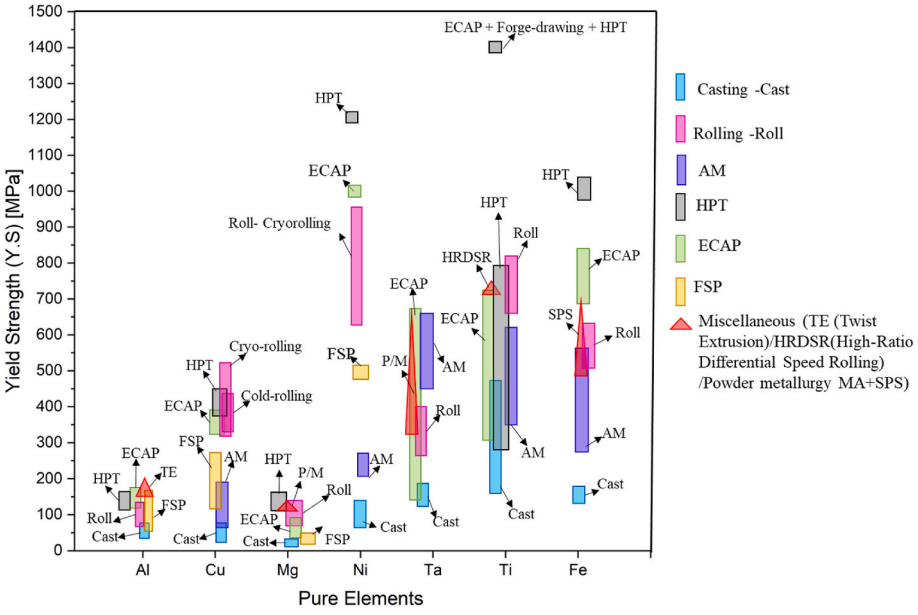

Fig. 3. Yield strength of pure elements obtained from various manufacturing processes (author's own contribution).

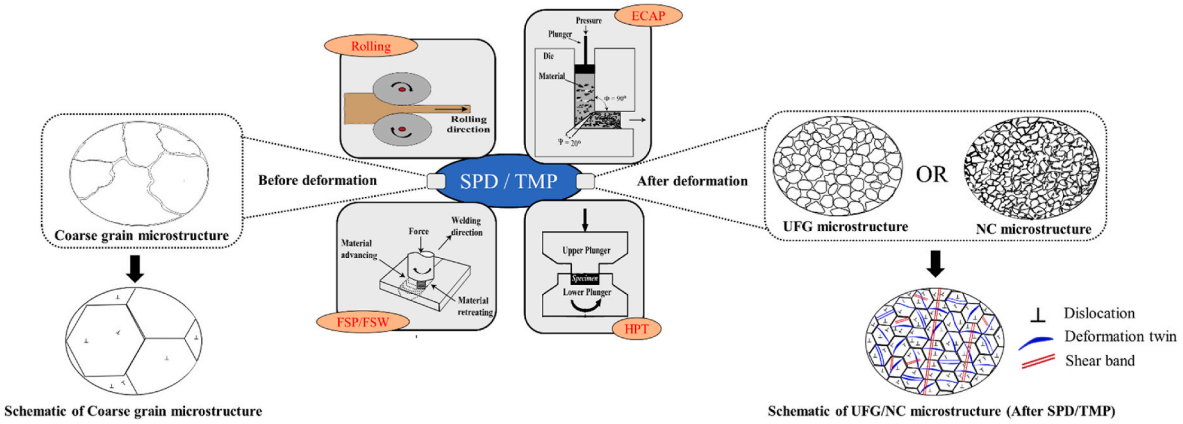

Fig. 4. Effect of TMP or SPD processes on the microstructure of an alloy (author's own contribution).

commercially pure (cp) Ti, the YS of HPT-processed samples ranged from 280 to 790 MPa [26–28]. However, the strength increased up to 1400 MPa when ECAP was performed at 450 °C (with an angle of 90°, route Bc, n = 8), followed by additional forge-drawing at 300 °C, reducing the diameter from 24 mm to 16 mm, prior to HPT. This combination of processes before HPT facilitated grain refinement and enhanced structural homogeneity, resulting in improved mechanical properties [32].

Achieving a balance of strength and ductility in MPEAs has been demonstrated through the creation of heterogeneous microstructure, combining ultrafine-grained (UFG) and larger elongated grains, or by inducing nanotwins and others [27]. Similarly, it has been proposed that the ductility of pure Cu can be enhanced by generating a bimodal microstructure (a combination of UFG and coarse grains) or by introducing twin boundaries [33]. Additionally, pure Mg processed via HPT also exhibits a bimodal microstructure both at 293 K and 423 K across 1/8, 1 and 10 turns. After 10 turns, the dislocation density was of the order of 3.26×10^{15} and 2.96×10^{14} at 293 K and 423 K respectively. This discrepancy arises from dislocation entanglements after rotations of 1/8 and 1 turn, with dynamic recrystallization initiating after 10 turns for the 293 K sample. In contrast, continuous dynamic recrystallization (CDRx) was evident throughout all turns for samples processed at 423 K. Consequently, samples produced at 293 K exhibit higher YS with moderate uniform elongation, while the samples produced at 423K showed relatively lower strength but large uniform elongation after 10 HPT turns [34]. The concepts of dislocation entanglements and continuous dynamic recrystallization (CDRx) are discussed in the following section.

1.2. Aspects of microstructural variations involved in strain engineering

1.2.1. Types of restoration mechanism during plastic deformation

A more fundamental question at this stage to answer is "How does the microstructure evolve during SPD or conventional TMP?" An answer to this question stems from fundamental materials science. Typically, when a material undergoes plastic deformation, a substantial number of dislocations are generated, leading to an increase of dislocation density. These dislocations then rearrange or annihilate, depending on the prevalent restoration mechanism. Dynamic recovery (DRV) and dynamic recrystallization (DRx) are the two crucial restoration mechanisms, which help to modify the microstructure by arranging dislocations during deformation. The three most critical microstructural features that define the microstructural evolution during deformation are grain size, grain shape (equiaxed or elongated/columnar) and grain boundary character distribution—such as low-angle grain boundaries (LAGBs) and high-angle grain boundaries (HAGBs).

During DRV, the mechanical properties of a deformed material are partially restored through rearrangement and annihilation of dislocations. As strain is experienced by the material, dislocation generation becomes more pronounced, leading to an increase in the dislocation density. Eventually, a steady state is reached whereby dislocation generation and annihilation balance each other, resulting in the formation of subgrains surrounded by low-angle grain boundaries (LAGBs). DRV primarily involves the migration of LAGBs inside the deformed grains and is typically observed in materials with high stacking fault energy (SFE) or those processed at lower temperatures (approximately 0.4 × Tm), facilitating the restoration of material properties.

Dynamic recrystallization (DRx) can be categorized into three types: discontinuous dynamic recrystallization (DDRx), continuous dynamic recrystallization (CDRx) and Geometric dynamic recrystallization (GDRx). The specific recrystallization mechanism depends on factors such as stacking fault energy (SFE), initial grain size and processing conditions.

DDRx is prevalent in materials with low stacking fault energy (SFE) during hot deformation, where nucleation of new strain-free grains occurs heterogeneously due to bulging of dislocations at grain-boundaries. In materials with low SFE, dislocations are unable to easily cross-slip, leading to the formation of a necklace-like structure at the grain boundaries. As deformation progresses, the strain-free nucleates start to grow at the expense of dislocations, migrating across the grain boundaries [35]. In certain cases, particularly during hot deformation, if the strain is halted after reaching a critical value without a reduction in temperature, the nuclei continue to grow using the stored energy. This phenomenon is referred to as post-dynamic recrystallization (PDRx) or metadynamic recrystallization (MDRx). In contrast to PDRx/MDRx, CDRx does not involve distinct nucleation and growth phases. Instead, it evolves the microstructure progressively, with subgrains surrounded by LAGBs transforming into grains enclosed by HAGBs as subgrains boundary misorientation increases at higher levels of deformation. CDRx is particularly prevalent in materials with high SFE, and can occur over a broad range of temperatures, from low to high-temperature deformation. GDRx is generally observed in materials with high SFE, undergoing deformation at elevated temperatures and large strain. During this process, HAGBs migrate, forming serrations with a wavelength comparable to the subgrain size. Significant grain elongation and thinning take place, and once the grain thickness reduces to below 1–2 subgrain sizes, the developed serrations pinch off, resulting in the formation of equiaxed grains with HAGBs. GDRx is especially common in materials with high SFE and is frequently observed during deformation to large strains with significant reduction in one direction, such as in hot rolling, where the original grains become elongated and refined [36].

The effect of other factors such as initial grain size and processing conditions has not been extensively studied for CDRx and GDRx, as these mechanisms of restoration of microstructure and mechanical properties were introduced later with the advent of SPD processes, hence not addressed in this study. However, it is important to emphasize that no definitive rule exists to determine which type of dynamic

recrystallization (DDRx, CDRx, or GDRx) will dominate under specific processing conditions [35]. For instance, CDRx can dominate in low SFE materials, as observed during the rolling of fine-grained 304 austenitic stainless steel [37]. Conversely, DDRx may occur in high-SFE materials, as reported in high-purity aluminum [38]. Moreover, depending on the processing conditions and initial grain size, these mechanisms can transition from one to another (e.g., from DDRx to CDRx) or even coexist simultaneously, as seen with the coexistence of CDRx and GDRx in Zircaloy-4 [39]. Consequently, generalizing the dominant restoration mechanism under given conditions remains a complex challenge.

1.2.2. Influence of material's microstructure

As the microstructure of a material evolves under plastic deformation, its mechanical properties also exhibit corresponding changes. The Hall-Petch relationship has long substantiated the influence of ultra-fine grained (UFG) and nano-crystalline (NC) structures on the mechanical properties of alloys. Materials deformed via SPD have consistently demonstrated enhanced YS, primarily due to their fine-grained structures (with grain sizes ranging from 200 nm to 1 μm), high dislocation density, and presence of nano-twins. Notably, HPT-processed materials exhibit exceptional strength, characterized by a significant fraction of HAGBs and grain sizes below 100 nm. Grain-boundary strengthening is well-described by the Hall-Petch relationship (see eq (1)) [40]. Kumar et al. [41], attributed the increased strength of FSP-processed $Al_{0.1}CoCrFeNi$ to a combination of grain boundary strengthening and lattice friction stress (commonly referred to as 'Peierls stress'), which is the force required to move a dislocation within the atomic plane of a unit cell [42,43]). Their observations of the gauge section of the tensile sample in the FSP-processed alloy revealed a distinct polycrystalline behavior, characterized by a significantly small grain size of 14 ± 10 μm, compared to the as-received sample's grain size of 500 μm. The reduction in grain size accommodated a larger number of grains, thereby amplifying the effectiveness of lattice friction stress and grain boundary strengthening mechanisms. In contrast, for the as-received sample, only the lattice friction stress contributed to YS, as the influence of grain boundaries was deemed negligible. It was further suggested that the contribution of dislocation strengthening to the YS could be considered negligible, given the low dislocation density present in the nugget microstructure after FSP [41].

Dislocation density plays a pivotal role in material strengthening, in contrast to the earlier notions that dislocations tend to weaken a material. In reality, a high dislocation density is highly desirable for improving strength. The strengthening due to dislocations can be quantitatively described using Taylor's equation, which correlates the increase in strength with dislocation density (see eq (2)) [40].

$$\sigma_y = \sigma_o + kd^{-1/2} \tag{1}$$

$$\sigma_y = \sigma_o + \alpha GbM\sqrt{\rho} \text{ where } \rho = \rho_0 + \rho_b \tag{2}$$

where σ_o is friction stress, k is the locking parameter, d is grain size, α is dislocation strength parameter, G is shear modulus, M is Taylor factor, b is Burgers vector, ρ is total dislocation density, ρ_0 is the dislocations present between the boundaries, and ρ_b is the GNDs contained within low angle boundaries.

In this context, dislocations can be categorized into two types: statistically stored dislocations (SSD) and geometrically necessary dislocations (GND). SSDs arise from random trapping during plastic deformation, while GNDs emerge in regions with high strain gradients ensuring geometrical compatibility and preventing the formation of overlaps and voids. GNDs are critical for accommodating localised deformation within the crystal structure. The presence of GNDs plays a significant role in influencing the flow stress of material, as described by the Taylor's model (see eq (2)).

In addition to the dislocations, mechanical twinning or deformation-induced twinning provides an alternative mechanism for accommodating plastic deformation in materials. Deformation twinning involves formation of mirror-image regions, known as twins, within a grain in response to shear stress. These twins introduce twin boundaries, acting as barriers to dislocation motion, thereby contributing to strengthening through grain refinement as described by the Hall-Petch hardening rule. Mechanical twinning was observed in HPT-deformed CoCrFeMnNi HEA [44], where the propensity of deformation caused an increase in twin density, along with the formation of new twin variants (micron-sized blocks of twin lamellae). At much higher strains (γ ranging from ~4.0 to ~50), the twin lamellae transformed, gradually diffusing into a homogeneous nano-crystalline (NC) structure. This demonstrated that deformation twinning can serve as a dominant mechanism for grain refinement (down to ~50 nm), resulting in exceptionally high strength accompanied by moderate ductility. Similarly, during plane-strain multi-pass rolling (ε = 80 %), conducted at both room and liquid nitrogen temperatures, deformation twinning was observed to be the primary strengthening mechanism. This led to a significant increase in UTS from 440 MPa to 1500 MPa at 77 K and 1200 MPa at 293 K, though at the cost of reduced ductility from original 71 % down to 12 % at 77 K and 14 % at 293K [45].

1.2.3. Other factors affecting materials strength

To understand the reasons why HPT leads to superior mechanical properties compared to other processing techniques, it's indispensable to understand the response of material under deformation or loading. In the subsequent section, the influence of crucial factors involved in different synthesis routes, the response of material under different deformation conditions and the mechanisms causing strengthening of materials have been discussed extensively.

The microstructure and mechanical properties of an alloy synthesized through various routes are influenced by several key factors. These include **cooling rate,** which is crucial in both casting and additive manufacturing (AM); the **applied pressure and temperature** during Hot-isostatic pressing (HIP) in powder metallurgy, where both parameters play a crucial role in determining density, porosity and microstructure. Conversely, in spark-plasma sintering (SPS), **temperature** predominantly governs the consolidation of powders. HIP typically results in higher density and finer microstructure compared to conventional sintering methods and is particularly advantageous for materials that are difficult to sinter. Additionally, factors such as **applied strain and processing temperature** during conventional-TMP and SPD techniques significantly influence the resulting microstructure and mechanical properties of an alloy.

The YS of additively manufactured alloys has demonstrated superior performance compared to cast samples, regardless of the elemental composition. This enhancement can be attributed to the rapid cooling rate during AM, which inhibits grain growth and promotes a finer microstructure. The typical cooling rates involved in casting and AM are presented in Table 1. However, despite the improved properties compared to as-cast alloys, the strength of additively manufactured alloys remains lower than those produced through conventional TMP and SPD methods. This disparity can be ascribed to several factors such as the formation of dendritic or columnar structures during layer-by-layer deposition, the introduction of residual stresses due to thermal gradients and rapid solidification, anisotropic mechanical properties, microstructural inhomogeneities, and porosity—particularly in powder-bed fusion techniques such as selective laser melting (SLM) and electron beam melting (EBM).

Table 1
Cooling rate during different processing techniques.

Processing route	Cooling Rate (K/s)
Casting	10^1–10^2 K/s [48–50]
Additive Manufacturing	10^2–10^8 K/s [48,51,52]

High-pressure torsion (HPT), Equal channel angular pressing (ECAP), Friction stir processing (FSP) and Twist extrusion (TE) are examples of SPD techniques, all of which fall under the "Top-down" approach, alongside conventional TMP methods such as rolling, forging and others. During "top-down" approach, bulk samples with a relatively coarse grain are subjected to substantial strain in order to refine the grain size, ultimately yielding ultrafine-grained (UFG) or a nanocrystalline (NC) structure [46]. Notably, this method mitigates the introduction of contaminants or porosity -common issues encountered during powder metallurgy (P/M) processes. Powder metallurgy itself contrarily employs a "bottom-up" approach; wherein bulk samples are fabricated by consolidating individual particles. This typically involves high-energy ball milling followed by consolidation techniques such as spark plasma sintering (SPS) or hot isostatic pressing (HIP) [46]. While this approach offers the advantage of producing fine microstructures, its applicability is often limited by challenges such as small size of finished products, the introduction of contaminants and residual porosity.

Conventional TMP methods, such as rolling, extrusion, drawing and forging are typically conducted at warm to hot temperatures to impart large strains while minimizing the risk of introducing defects such as cracks. This is because these processes primarily apply uniaxial compressive stress, which at ambient temperatures often lead to formation of various defects. In contrast, non-conventional TMP or SPD methods impart significant strain without inducing cracking by utilizing a combination of compressive stress (to prevent cracking) and shear stress (to introduce large strain). Furthermore, one of the key advantages of SPD techniques is their ability to impose large plastic strains on a material without altering its overall shape; that is, the material retains its initial geometry after the SPD process [47]. Strains of several hundred to thousands of percent can be achieved during SPD processes. For instance, during ECAP, a material is subjected to multiple passes through a die with intersecting channels, leading to cumulative strain with each pass. Similarly, in HPT, the material undergoes torsional deformation under high pressure, resulting in substantial strain accumulation. Table 2 provides an overview of the typical strain rates (sec^{-1}) associated with various manufacturing processes.

Strain rate ($\dot{\mathscr{E}}$) refers to the time dependent strain or the rate at which deformation occurs in a material. Though, it quantifies the rate of deformation but does not reflect the cumulative strain or deformation imparted to the material during processing.

Effective plastic strain ($\mathscr{E}_{eff}$) is a key parameter that quantifies the cumulative permanent deformation that the material experiences during its deformation process. Unlike strain rate, which is measured in sec^{-1}, effective plastic strain is a dimensionless quantity and is calculated by integrating the plastic strain over the entire deformation cycle. The calculation of $\mathscr{E}_{eff}$ is governed by Equation (3), with specific formulations for the ECAP and HPT processes represented by Equations (4) and (5), respectively [33].

$$\mathscr{E}_{eff} = \left\{ \frac{2}{9}\left[(\mathscr{E}_{11} - \mathscr{E}_{22})^2 + (\mathscr{E}_{22} - \mathscr{E}_{33})^2 + (\mathscr{E}_{33} - \mathscr{E}_{11})^2 \right] + \frac{1}{3}\left(\gamma_{12}^2 + \gamma_{23}^2 + \gamma_{31}^2\right) \right\}^{0.5} \tag{3}$$

$$\mathscr{E}_{eff} = \frac{1}{\sqrt{3}}\left[2\cot\left(\frac{\Phi + \Psi}{2}\right) + \Psi\, cosec\left(\frac{\Phi + \Psi}{2}\right) \right] \tag{4}$$

$$\boldsymbol{\gamma} = \frac{2\pi r N}{t} \tag{5}$$

where Φ is the inner angle/oblique angle/channel angle, Ψ is the outer angle/corner angle, $\boldsymbol{\gamma}$ is the shear strain along the radius (r), N is the number of rotations and t is thickness of the disk.

Table 3 illustrates the extent of effective plastic strain induced in various manufacturing processes. During rolling, which is a conventional TMP method, the effective plastic strain of 0.8 results in 50 % reduction in height, while it reaches 2.66 for a 90 % reduction in height [33]. For the most common inner angle (Φ = 90°) and outer angle (Ψ = 20°) in a single ECAP pass, the effective plastic strain value is 1. For N such passes, the total imposed effective plastic strain becomes N. By varying the inner and outer angles, the amount of effective plastic strain induced can be adjusted. For instance, with Φ = 90° and Ψ = 0°, the effective plastic strain per pass increases to 1.15 [33]. The HPT process induces a broad range of effective plastic strain, from a minimum of 8 to a maximum of 20. This significant capacity for imparting high levels of effective plastic strain is a key factor contributing to the superior YS of materials processed via HPT, compared to those subjected to other manufacturing techniques. The extent of effective plastic strain across various manufacturing processes is schematically represented in Fig. 5.

Fig. 6 demonstrates the effectiveness of employing SPD processing over conventional methods. SPD-processed components have been observed to offer exceptional mechanical properties such as increased strength and toughness. For instance, Sadasivan & Balasubramanian [57] reviewed various SPD techniques used for processing tubular materials, which are among the most widely used industrial products. They emphasized that SPD-processed tubes, with strengthened walls, can be produced with reduced thickness, leading to material savings and contributing to sustainability. Moreover, components processed via SPD demonstrate improves fatigue life, corrosion resistance, and wear resistance compared to those produced through conventional methods. This can reduce the frequency of replacements and repairs, resulting in cost savings and supporting the development of more sustainable

Table 2
Strain rate during different processing techniques.

Processing route	Strain rate (sec^{-1})
Rolling (Plane strain compression)	10^1 to 8×10^2 (depending on the working temperature and thickness reduction) [53]
ECAP	10^{-3} to 10^0 (depending on the corner and channel angle) [54]
HPT	10^{-2} to 2×10^1 (depending on the pressure, rotation speed and number of turns) [55]
Powder metallurgy	–

Table 3
Effective plastic strain during different processing techniques.

Processing route	Effective plastic strain
Uniaxial compression (UC)	0.69 (50 % reduction in height) - 2.30 (90 % reduction in height) [33]
Rolling (Plane strain compression)	0.80 (50 % reduction in height) - 2.66 (90 % reduction in height) [33]
ECAP	1.15 (Φ (oblique angle (or channel angle)) = 90° and Ψ (corner angle) = 0°). For more common angle of Φ = 90° and Ψ = 20°, ε_{eff} = 1; for N such passes, the total ε_{eff} will be N [33].
HPT	effective plastic strains of about 8–10, and in some cases up to 20 [33].
Powder Metallurgy (P/M)	effective plastic strains of about 0.01–0.1 per pass during powder compaction [56].

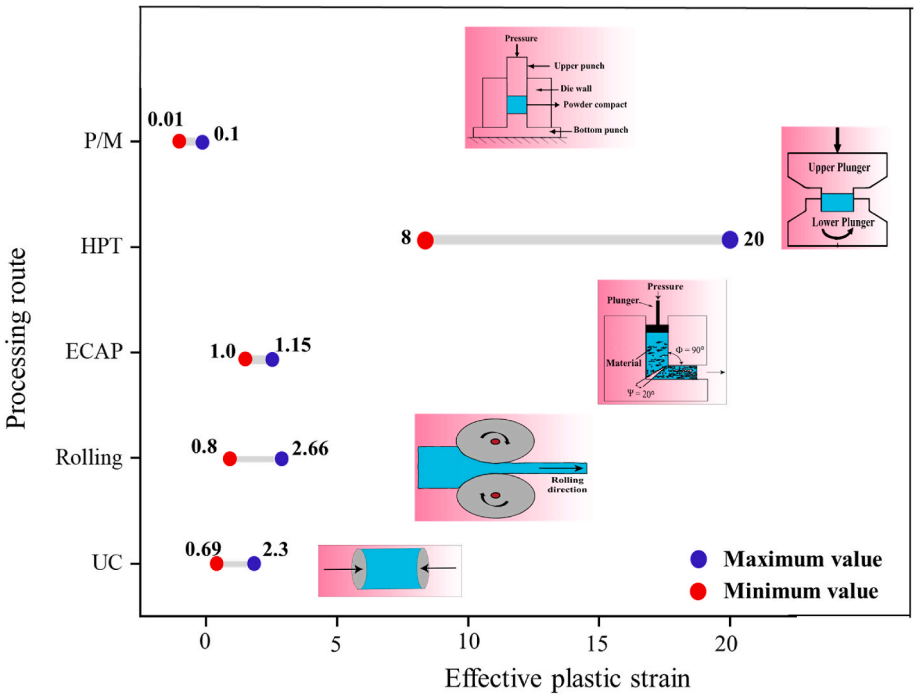

Fig. 5. Effective plastic strain during different processing techniques. P/M: Powder Metallurgy; HPT: High Pressure Torsion; ECAP: Equal Channel Angular Pressing; UC: Uniaxial Compression (author's own contribution).

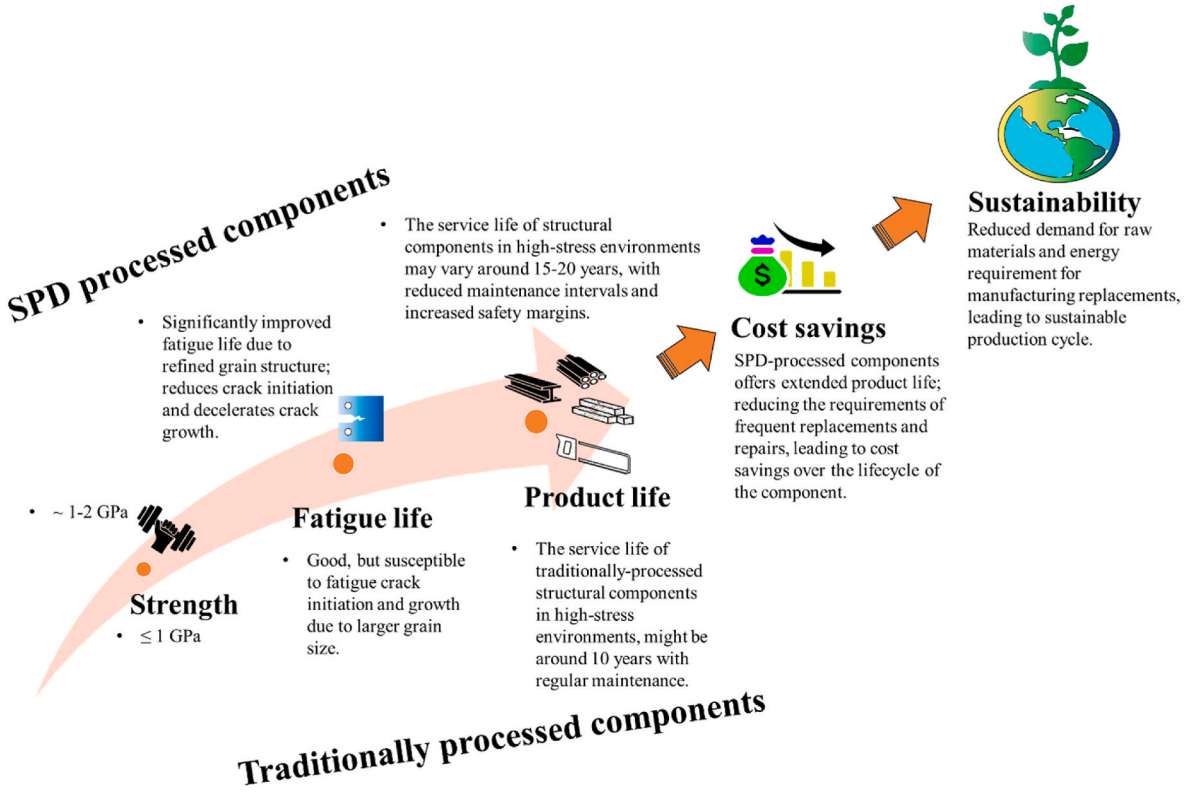

Fig. 6. Cost-effectiveness of using SPD over traditional-processing routes (author's own contribution).

products with lower carbon emissions. SPD techniques have also been employed to fabricate high-strength components, such as micro-bolts from UFG carbon steel [58], turbine blades from AA6063 [59], and high-strength bolts from AA6061 [60], using hybrid processes such as drawing, ECAP, and rolling.

2. Concluding remarks

This study highlights the critical importance of strain engineering as a timely and effective approach to reduce reliance on strategic and critical raw materials (S&CRMs) in the development of high-

performance metallic alloys. Strain engineering enables precise control over key microstructural parameters, such as grain size, grain structure, nanotwin formation, and activation of deformation mechanisms like twinning/transformation-induced plasticity (TWIP/TRIP). These mechanisms enhance mechanical properties that would otherwise require modifications in material composition involving S&CRMs.

We have demonstrated that strain engineering provides a viable path for creating sustainable alloys, particularly for demanding applications. For instance, hydrogen storage materials processed by high-pressure torsion (HPT) to produce ultrafine-grained (UFG) structures outperform those processed through conventional methods such as thermal annealing, groove rolling, and high-energy ball milling [61]. UFG pure titanium (higher grade) exhibits a higher fatigue limit and improved properties for bioimplant applications compared to traditional Ti6Al4V alloys [62–65]. Furthermore, the introduction of nanotwins via severe plastic deformation (SPD) in UFG microstructures enhances strength without compromising electrical conductivity, making them excellent alternatives to copper alloys for electrical applications requiring higher strength. These findings suggest that SPD techniques could pave the way for a new class of high-performance, sustainable materials suited to various industrial applications, including bioimplants, electrical components, and structural engineering.

Additionally, strain-engineered materials often require reduced thickness due to their improved mechanical properties, leading to weight savings, lower fuel consumption in transportation, and reduced storage needs. Their superior fatigue life, corrosion resistance, and wear resistance extend longevity and minimise the need for frequent repairs and replacements. This supports sustainability goals by reducing carbon emissions, a key step towards achieving Net-Zero targets.

In conclusion, this research opens promising avenues for further exploration, particularly in optimizing SPD techniques for scalable industrial production. The development of S&CRM-free or reduced-S&CRM alloys through strain engineering could significantly lessen dependence on rare earth materials to reduce energy in their carbon-intensive mining, thus directly contributing to more sustainable metal processing. This study not only showcases the current capabilities of strain engineering but also underscores its potential to transform material design, sustainability, and technological innovation steps that needs to be initiated across industries around the world.

Declaration of generative AI and AI-assisted technologies in the writing process

During the preparation of this work the author(s) used AI assistance to improve the readability and language of the manuscript. The authors reviewed and edited the final content and took full responsibility for the content of the published article.

CRediT authorship contribution statement

Swati Singh: Writing – original draft. **Mingwen Bai:** Software. **Allan Matthews:** Writing – review & editing. **Shrikrishna N. Joshi:** Writing – review & editing. **Saurav Goel:** Writing – review & editing.

Declaration of competing interest

The authors declare that they have no known competing financial interests or personal relationships that could have appeared to influence the work reported in this paper.

Acknowledgment(s)

SNJ would like to thank the Department of Science and Technology (DST) India. SG would like to acknowledge financial support from the UKRI via Grant No. EP/T024607/1. We also acknowledge the Royal Society Research Grant (RGS\R2\222304) for funding the purchase of Thermo-Calc software and database (TCHEA6 and MOBHEA2 for High Entropy Alloys).

Appendix A. Supplementary data

Supplementary data to this article can be found online at https://doi.org/10.1016/j.mtadv.2024.100538.

Data availability

Data will be made available on request.

References

[1] P. Ji, et al., Exceptional strength–ductility combination of CoCrFeMnNi high-entropy alloy with fully recrystallized structure by selective laser melting after post-deformation annealing, J. Mater. Res. Technol. 23 (2023) 3166–3176.
[2] D. Li, et al., High-entropy Al0. 3CoCrFeNi alloy fibers with high tensile strength and ductility at ambient and cryogenic temperatures, Acta Mater. 123 (2017) 285–294.
[3] S. Wang, et al., Mechanical instability and tensile properties of TiZrHfNbTa high entropy alloy at cryogenic temperatures, Acta Mater. 201 (2020) 517–527.
[4] J. Chen, et al., A review on fundamental of high entropy alloys with promising high–temperature properties, J. Alloys Compd. 760 (2018) 15–30.
[5] S. Praveen, H.S. Kim, High-entropy alloys: potential candidates for high-temperature applications–an overview, Adv. Eng. Mater. 20 (1) (2018) 1700645.
[6] W. Yang, et al., Design and properties of novel Ti–Zr–Hf–Nb–Ta high-entropy alloys for biomedical applications, Intermetallics 141 (2022) 107421.
[7] Y. Ma, et al., High-entropy energy materials: challenges and new opportunities, Energy Environ. Sci. 14 (5) (2021) 2883–2905.
[8] S. Manfredi, et al., Raw Materials Information System (RMIS): towards V2. 0, 2017.
[9] E. Commission, Tackling the Challenges in Commodity Markets and on Raw Materials, European Commission, Brussels, 2011.
[10] E. Commission, On the review of the list of critical raw materials for the EU and the implementation of the raw materials initiative. Ad-hoc Working Group on Defining Critical Raw Minerals of the Raw Materials Supply Group, 2014.
[11] E. Commission, List of Critical Raw Materials for the EU, Online verfügbar unter, 2017.
[12] E. Commission, Critical Raw materials resilience: charting a path towards greater security and sustainability. Communication from the Commission to the European Parliament, the Council, the European Economic and Social Committee and the Committee of the Regions, 2020.
[13] M. Grohol, C. Veeh, Study on the Critical Raw Materials for the EU 2023, Publications Office of the European Union, 2023.
[14] G. Salishchev, et al., Effect of Mn and V on structure and mechanical properties of high-entropy alloys based on CoCrFeNi system, J. Alloys Compd. 591 (2014) 11–21.
[15] J. He, et al., Effects of Al addition on structural evolution and tensile properties of the FeCoNiCrMn high-entropy alloy system, Acta Mater. 62 (2014) 105–113.
[16] H. Shahmir, et al., Effect of annealing on mechanical properties of a nanocrystalline CoCrFeNiMn high-entropy alloy processed by high-pressure torsion, Mater. Sci. Eng., A 676 (2016) 294–303.
[17] P. Sathiyamoorthi, et al., Effect of annealing on microstructure and tensile behavior of CoCrNi medium entropy alloy processed by high-pressure torsion, Entropy 20 (11) (2018) 849.
[18] B. Schuh, R. Pippan, A. Hohenwarter, Tailoring bimodal grain size structures in nanocrystalline compositionally complex alloys to improve ductility, Mater. Sci. Eng., A 748 (2019) 379–385.
[19] P. Sathiyamoorthi, et al., Superior cryogenic tensile properties of ultrafine-grained CoCrNi medium-entropy alloy produced by high-pressure torsion and annealing, Scripta Mater. 163 (2019) 152–156.
[20] D. Xu, et al., A critical review of the mechanical properties of CoCrNi-based medium-entropy alloys, Microstructures 2 (1) (2022) 2022001.
[21] F. Otto, et al., The influences of temperature and microstructure on the tensile properties of a CoCrFeMnNi high-entropy alloy, Acta Mater. 61 (15) (2013) 5743–5755.
[22] B. Gludovatz, et al., Exceptional damage-tolerance of a medium-entropy alloy CrCoNi at cryogenic temperatures, Nat. Commun. 7 (1) (2016) 10602.
[23] Y. Wang, et al., High tensile ductility in a nanostructured metal, nature 419 (6910) (2002) 912–915.
[24] Y.H. Zhao, et al., Simultaneously increasing the ductility and strength of ultra-fine-grained pure copper, Adv. Mater. 18 (22) (2006) 2949–2953.
[25] L. Lu, et al., Ultrahigh strength and high electrical conductivity in copper, Science 304 (5669) (2004) 422–426.
[26] Y. Tian, et al., Enhanced strength and ductility in an ultrafine-grained Fe-22Mn-0.6 C austenitic steel having fully recrystallized structure, Metall. Mater. Trans. 45 (2014) 5300–5304.
[27] S. Picak, H. Yilmaz, I. Karaman, Simultaneous deformation twinning and martensitic transformation in CoCrFeMnNi high entropy alloy at high temperatures, Scripta Mater. 202 (2021) 113995.
[28] A. Mohammadi, et al., High strength and high ductility of a severely deformed high-entropy alloy in the presence of hydrogen, Corrosion Sci. 216 (2023) 111097.

[29] M. Koyama, K. Ichii, K. Tsuzaki, Grain refinement effect on hydrogen embrittlement resistance of an equiatomic CoCrFeMnNi high-entropy alloy, Int. J. Hydrogen Energy 44 (31) (2019) 17163–17167.
[30] B. Schuh, et al., Thermodynamic instability of a nanocrystalline, single-phase TiZrNbHfTa alloy and its impact on the mechanical properties, Acta Mater. 142 (2018) 201–212.
[31] N. Maury, et al., A critical examination of pure tantalum processed by high-pressure torsion, Mater. Sci. Eng., A 638 (2015) 174–182.
[32] R. Islamgaliev, et al., Microstructure and mechanical properties of titanium (Grade 4) processed by high-pressure torsion, Mater. Sci. Eng., A 493 (1–2) (2008) 190–194.
[33] R. Kapoor, Severe plastic deformation of materials, in: Materials under Extreme Conditions, Elsevier, 2017, pp. 717–754.
[34] Z. Li, et al., An evaluation of the mechanical properties, microstructures, and strengthening mechanisms of pure Mg processed by high-pressure torsion at different temperatures, Adv. Eng. Mater. 24 (10) (2022) 2200799.
[35] K. Huang, R.E. Logé, A review of dynamic recrystallization phenomena in metallic materials, Mater. Des. 111 (2016) 548–574.
[36] T. Sakai, et al., Dynamic and post-dynamic recrystallization under hot, cold and severe plastic deformation conditions, Prog. Mater. Sci. 60 (2014) 130–207.
[37] Z. Yanushkevich, A. Belyakov, R. Kaibyshev, Microstructural evolution of a 304-type austenitic stainless steel during rolling at temperatures of 773–1273 K, Acta Mater. 82 (2015) 244–254.
[38] H. Yamagata, et al., Nucleation of new grains during discontinuous dynamic recrystallization of 99.998 mass% Aluminum at 453 K, Scripta Mater. 45 (9) (2001) 1055–1061.
[39] C. Chauvy, P. Barberis, F. Montheillet, Microstructure transformation during warm working of β-treated lamellar Zircaloy-4 within the upper α-range, Mater. Sci. Eng., A 431 (1–2) (2006) 59–67.
[40] H. Lanjewar, L.A. Kestens, P. Verleysen, Damage and strengthening mechanisms in severely deformed commercially pure aluminum: experiments and modeling, Mater. Sci. Eng., A 800 (2021) 140224.
[41] N. Kumar, et al., Friction stir processing of a high entropy alloy Al 0.1 CoCrFeNi, Jom 67 (2015) 1007–1013.
[42] F.R.N. Nabarro, Theoretical and experimental estimates of the Peierls stress, Philos. Mag. A 75 (3) (1997) 703–711.
[43] B. Joos, M. Duesbery, The Peierls stress of dislocations: an analytic formula, Phys. Rev. Lett. 78 (2) (1997) 266.
[44] B. Schuh, et al., Mechanical properties, microstructure and thermal stability of a nanocrystalline CoCrFeMnNi high-entropy alloy after severe plastic deformation, Acta Mater. 96 (2015) 258–268.
[45] N. Stepanov, et al., Effect of cryo-deformation on structure and properties of CoCrFeNiMn high-entropy alloy, Intermetallics 59 (2015) 8–17.
[46] L. Kecskes, et al., Grain size engineering of bcc refractory metals: top-down and bottom-up—application to tungsten, Mater. Sci. Eng., A 467 (1–2) (2007) 33–43.
[47] J. Wongsa-Ngam, M. Kawasaki, T.G. Langdon, A comparison of microstructures and mechanical properties in a Cu–Zr alloy processed using different SPD techniques, J. Mater. Sci. 48 (2013) 4653–4660.
[48] S. Shakil, et al., Additive manufactured versus cast AlSi10Mg alloy: microstructure and micromechanics, Results in Materials 10 (2021) 100178.
[49] P. Pawlik, K. Pawlik, A. Przybył, Investigation of the cooling rate in the suction casting process, Rev. Adv. Mater. Sci. 18 (1) (2008) 81.
[50] J.-C. Zhao, M.R. Notis, Continuous cooling transformation kinetics versus isothermal transformation kinetics of steels: a phenomenological rationalization of experimental observations, Mater. Sci. Eng. R Rep. 15 (4–5) (1995) 135–207.
[51] B. Chen, et al., Strength and strain hardening of a selective laser melted AlSi10Mg alloy, Scripta Mater. 141 (2017) 45–49.
[52] P. Cheng, et al., Microstructural evolution and mechanical properties of Al0.3CoCrFeNiSix high-entropy alloys containing coherent nanometer-scaled precipitates, Mater. Sci. Eng., A 772 (2020) 138681.
[53] H. Yada, et al., Strength and structural changes under high strain-rate hot deformation of C steels, Transactions of the Iron and Steel Institute of Japan 23 (2) (1983) 100–109.
[54] H.S. Kim, Evaluation of strain rate during equal-channel angular pressing, J. Mater. Res. 17 (1) (2002) 172–179.
[55] K. Edalati, et al., Significance of strain rate in severe plastic deformation on steady-state microstructure and strength, Mater. Sci. Eng., A 859 (2022) 144231.
[56] L. Akhmetshin, I.Y. Smolin, S.P. Buyakova, Numerical study of hard-metal powder compaction, in: IOP Conference Series: Materials Science and Engineering, IOP Publishing, 2021.
[57] N. Sadasivan, M. Balasubramanian, Severe plastic deformation of tubular materials–Process methodology and its influence on mechanical properties–A review, Mater. Today: Proc. 46 (2021) 3460–3468.
[58] A. Yanagida, K. Joko, A. Azushima, Formability of steels subjected to cold ECAE process, J. Mater. Process. Technol. 201 (1–3) (2008) 390–394.
[59] D. Salcedo, et al., Manufacturing of nanostructured blades for a Francis turbine by isothermal forging of AA6063, J. Manuf. Sci. Eng. 136 (1) (2014) 011009.
[60] J.H. Kim, et al., High-strength bolt-forming of fine-grained aluminum alloy 6061 with a continuous hybrid process, Mater. Sci. Eng., A 552 (2012) 316–322.
[61] K. Edalati, E. Akiba, Z. Horita, High-pressure torsion for new hydrogen storage materials, Sci. Technol. Adv. Mater. 19 (1) (2018) 185–193.
[62] M. Fattahi, et al., Severe plastic deformation: nanostructured materials, metal-based and polymer-based nanocomposites: a review, Helliyon 9 (12) (2023) e22559.
[63] R.Z. Valiev, Superior strength in ultrafine-grained materials produced by SPD processing, Mater. Trans. 55 (1) (2014) 13–18.
[64] A. Medvedev, et al., Comparison of laboratory-scale and industrial-scale equal channel angular pressing of commercial purity titanium, Mater. Lett. 145 (2015) 308–311.
[65] C.N. Elias, et al., Ultrafine grained titanium for biomedical applications: an overview of performance, J. Mater. Res. Technol. 2 (4) (2013) 340–350.